Int. J. Heat Mass Transfer. Vol. 20, pp. 409–419. Pergamon Press 1977. Printed in Great Britain

VOID FRACTION AND INCIPIENT POINT OF BOILING DURING THE SUBCOOLED NUCLEATE FLOW BOILING OF WATER

H. C. ÜNAL
Central Technical Institute TNO, P.O. Box 342, Apeldoorn, The Netherlands

(*Received* 12 *May* 1976)

Abstract—Void fraction has been determined with high-speed photography for subcooled nucleate flow boiling of water. The data obtained and the data of various investigators for adiabatic flow of stream–water mixtures and saturated bulk boiling of water have yielded a correlation which covers the following conditions: geometry: vertically orientated circular tubes, rectangular channels and annuli; pressure: 2–15.9 MN/m^2; mass velocity: 388–3500 $kg/m^2 s$; void fraction: 0–99%; hydraulic diameter: 0.0047–0.0343 m; heat flux: adiabatic and 0.01–2.0 MW/m^2. The accuracy of the correlation is estimated to be 12.5%.

The value of the so-called distribution (or flow) parameter has been experimentally determined and found to be equal to 1 for a vertical small-diameter circular tube.

The incipient point of boiling for subcooled nucleate flow boiling of water has been determined with high-speed photography. The data obtained and the data available in the literature have yielded a correlation which covers the following conditions: geometry: plate, circular tube and inner tube-heated, outer tube-heated and inner- and outer tube heated annulus; pressure: 0.15–15.9 MN/m^2; mass velocity: 470–17355 $kg/m^2 s$; hydraulic diameter: 0.00239–0.032 m; heat flux: 0.13–9.8 MW/m^2; subcooling: 2.6–108 K; material of heating surface: stainless steel and nickel. The accuracy of the correlation is estimated to be 27.5%.

Maximum bubble diameters have been measured at the incipient point of boiling. These data and the data from literature have been correlated for the pressure range of 0.1–15.9 MN/m^2.

NOMENCLATURE

A, cross-sectional area [m^2];
C, distribution parameter;
c, specific heat capacity of material of heating surface [J/kg K];
c_p, specific heat capacity at constant pressure [J/kg K];
C_1, constant, defined by equation (32) [$W/m^2 K^n$];
D, bubble or plug diameter [m];
D_d, maximum bubble diameter [m];
d, pipe diameter [m];
d_H, hydraulic diameter [m];
d_1, inner diameter of annulus [m];
d_2, outer diameter of annulus [m];
e, total number of plugs and bubbles in test section;
f, number of bubbles in a sample;
G, mass velocity [$kg/m^2 s$];
g, acceleration of gravity [m/s^2];
H, enthalpy [J/kg];
h, single-phase forced convection heat-transfer coefficient [$W/m^2 K$];
J, volume flux density [m/s];
$\bar{J}$, average volumetric flux density of a two-phase mixture, defined by equation (11) [m/s];
K, flow parameter;
k, thermal conductivity [W/mK];
m, number of axial positions;
Nu, Nusselt number;
n, constant, defined by equation (32);
P, pressure [N/m^2];
P_c, critical pressure [N/m2];
P_r, reduced pressure, $P_r = P/P_c$;
Pr, Prandtl number;
Q, volumetric flow rate [m^3/s];
q, heat flux [W/m^2];
Re, Reynolds number;
r, latent heat of evaporation [J/kg];
S, slip ratio;
T, temperature on water side [K];
ΔT_{sat}, superheating on water side (i.e. difference between wall temperature and saturation temperature of the liquid) [K];
ΔT_{sub}, subcooling on water side (i.e. difference between saturation temperature and bulk liquid temperature) [K];
t, temperature on sodium side [K];
U, over-all coefficient of heat transfer [$W/m^2 K$];
u, liquid bulk velocity [m/s];
V, instantaneous bubble or plug velocity [m/s];
V_d, weighted mean drift velocity, defined by equation (13) [m/s];
V_v, velocity of vapour phase [m/s];
$\bar{V}$, weighted mean velocity of vapour phase, defined by equations (10), (18) and (19) [m/s];
v_d, drift velocity, defined by equation (14) [m/s];

$\bar{v}_1$, mean velocity of the vapour phase, defined by equation (2) [m/s]; equation (2) [m/s];
$\bar{v}_2$, mean velocity of the liquid phase, defined by equation (3) [m/s];
W, mass flow [kg/s];
X, steam quality;
Y, variable.

Greek symbols
α, void fraction;
$\bar{\alpha}$, void fraction, average over cross-section;
β, vapour volumetric rate ratio, defined by equation (5);
μ, dynamic viscosity [kg/m²s];
ρ, density [kg/m³];
σ, surface tension [N/m].

Subscripts
b, refers to bulk condition;
F, refers to condition for pool boiling or fully developed boiling;
I, refers to condition for incipient point of boiling;
i, refers to inlet condition;
L, refers to liquid phase;
l, refers to saturation condition for liquid phase;
n, refers to sodium side;
o, refers to outlet condition;
s, refers to heated surface or material of heated surface;
v, refers to vapour phase;
w, refers to water/steam side;
z, refers to axial position at 9 m along the test pipe.

1. VOID FRACTION—INTRODUCTION

THE DETERMINATION of void fraction is of practical importance for the design of steam generators and liquid-cooled reactors.

The best known equation used to determine void fraction is the so-called slip correlation, which, in fact, is a physical definition of the slip ratio:

$$S = \frac{\bar{v}_1}{\bar{v}_2} = \frac{X}{1-X}\,\frac{1-\bar{\alpha}}{\bar{\alpha}}\,\frac{\rho_L}{\rho_v} \tag{1}$$

where

$$\bar{v}_1 = \frac{Q_v}{A_v} = \frac{XW}{\rho_v A_v} \tag{2}$$

$$\bar{v}_2 = \frac{Q_L}{A_L} = \frac{(1-X)W}{\rho_L A_L}. \tag{3}$$

$\bar{\alpha}$ is, per definition, equal to A_v/A.

An other type of equation used for the determination of void fraction is from Armand [1]:

$$\beta/\bar{\alpha} = \frac{1}{K} = C \tag{4}$$

where

$$\beta = \frac{Q_v}{Q_v+Q_L} = \frac{X}{X+(1-X)(\rho_v/\rho_L)}. \tag{5}$$

Armand has experimentally demonstrated that the flow parameter K in equation (4) is a constant for adiabatic bubble and slug flow of air–water mixtures in a horizontal pipe at atmospheric pressure conditions for vapour volumetric ratios of less than 0.9 and greater than 0.3. Later Armand and Treshchev [2] have shown indirectly that the flow parameter is a pressure-dependent constant for the flow of steam–water mixtures with or without heat addition in horizontal pipes for the pressure range of 0.98–17.7 MN/m² and for steam qualities less than 0.9. Bankoff [3] was the first to derive equation (4), and evaluate theoretically the flow parameter by assuming a power-law distribution for both radial velocity and void fraction for bubble flow in a circular tube. He has verified equation (4) using data for steam–water mixtures with or without heat addition obtained in vertically and horizontally orientated rectangular channels and circular tubes up to 13.8 MN/m². He reports that the flow parameter is a pressure-dependent constant. Owing to the lack of data, however, he was not able to show directly whether the flow parameter he evaluated theoretically is a pressure-dependent constant. Bankoff has related the slip ratio to the flow parameter as given below:

$$S = \frac{\bar{v}_1}{\bar{v}_2} = \frac{1-\bar{\alpha}}{K-\bar{\alpha}}. \tag{6}$$

Zuber and Findlay [4] have derived a general expression to determine velocity field and void fraction in any two-phase flow by considering radial void- and volume flux density distributions and the relative between the two phases in a channel:

$$\bar{V}/\bar{J} = C + V_d/\bar{J} \tag{7}$$

$$\bar{V}/\bar{J} = \beta/\bar{\alpha} \tag{8}$$

and therefore

$$\beta/\bar{\alpha} = C + V_d/\bar{J} \tag{9}$$

where

$$\bar{V} = \frac{\langle V_v \alpha \rangle}{\langle \alpha \rangle} \tag{10}$$

$$\bar{J} = \frac{Q_L + Q_v}{A} = G\left(\frac{X}{\rho_v} + \frac{1-X}{\rho_L}\right) \tag{11}$$

$$C = \frac{\langle \alpha J \rangle}{\langle \alpha \rangle \langle J \rangle} \tag{12}$$

$$V_d = \frac{\langle v_d \alpha \rangle}{\langle \alpha \rangle} \tag{13}$$

$$v_d = V_v - J. \tag{14}$$

The $\langle\,\rangle$'s denote averages over the cross-section defined by equation

$$\langle Y \rangle = \frac{\int Y \,\mathrm{d}A}{A}. \tag{15}$$

The aforesaid investigators have evaluated the distribution parameter C in equation (9) for a circular tube by assuming a polinomial distribution for profiles of radial void- and volume flux density. It is reported in [4–7] that, in general, this parameter is a function of flow pattern and geometry, and that V_d, the weighted mean drift velocity in equation (9), is a function of flow pattern, geometry and pressure.

Zuber *et al.* [6] and Staub and Zuber [5] have shown that equation (9) well correlates water and Refrigerant-22 data taken in vertical circular tubes and rectangular channels and over a large range of conditions if the effects of flow regimes and geometry are not considered, i.e.

$$C = 1.13 \tag{16}$$

$$V_d = 1.18[\sigma g(\rho_L - \rho_v)/\rho_L^2]^{1/4}. \tag{17}$$

Although Zuber *et al.* [6] have directly shown that the distribution parameter calculated with profiles of void fraction and volume flux density as measured by Adorni *et al.* [8] in a circular tube is about 1.14, the weighted mean drift velocity evaluated from the same data (Fig. 1 in [6]) differs by about 1270% from that evaluated from equation (17).

It has not been demonstrated directly in [4–6] that equation (8) and therefore equation (7) is also valid.

When the relative velocity between the two phases is zero or negligible, as in the case of the flow in horizontal channels or flow in vertical pipes at high velocities and elevated pressures (see equations (9) and (17)), the weighted mean drift velocity, or V_d/J in equation (9), becomes zero or negligible, and equation (9) reduces to equation (4). In this case the values of the distribution (or flow) parameter reported by Armand and Treshchev [2], Bankoff [3] and Zuber *et al.* [6] are in serious disagreement with each other. Furthermore the radial void distribution measured recently with an advanced technique by Inoue *et al.* [9], Kobayasi [10] and Ohba [11] for the bubble flow regime in a circular tube and in a rectangular channel deviates considerably from that assumed by Zuber and Findlay [4], Zuber *et al.* [6] and Bankoff [2] to predict the distribution (or flow) parameter.

It follows from the above discussion that adequate data are needed for the value of the distribution parameter and the weighted mean drift velocity. As indicated in [4], equation (7) gives a straight line with slope C in the $\bar{V}/J$-plane and the interception of this line with the $\bar{V}$-axis gives the value of the weighted mean drift velocity. For the determination of equation (7) for a given flow regime and pressure, therefore, it is sufficient to measure the weighted mean velocity of the vapour phase for at least two given sets of operating conditions (i.e. mass velocity, steam quality and subcooling) in a channel since J, the average volumetric flux density of the mixture, depends only on the operating conditions.

The purpose of the first part of this paper is to demonstrate the experimental determination of equation (7) for bubble- and plug flow in a vertical small-diameter pipe, and subsequently show the validity of equation (8) and therefore of equation (9).

A correlation is also presented to predict the void fraction for the subcooled nucleate flow boiling of water, the saturated bulk boiling of water and the flow of steam–water mixtures without heat addition in vertical channels. Subcooled nucleate flow boiling is also referred to as "partial nucleate boiling", "forced convection surface-boiling" or simply as "surface boiling" in literature.

EXPERIMENTAL SET-UP

The experimental set-up has been described in detail elsewhere [12, 13]. The photographical test section was an adiabatic, cylindrical sapphire of 8 mm I.D. and 20 mm height, mounted just at the end of a 10 m long sodium heated test pipe, as shown in Fig. 1. This test

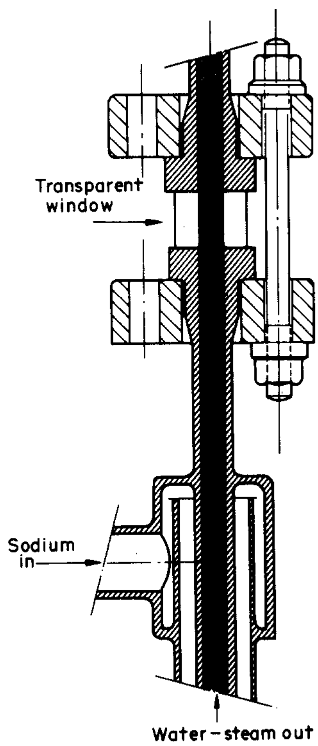

FIG. 1. Top part of test pipe with cylindrical sapphire test section.

pipe has been installed in a loop, of which the flow diagram is given in Fig. 2. The high-pressure part of the Loop has been drawn in thick lines and the low-pressure part in thin lines. Both the test pipe and the Loop have been constructed from stainless steel, grade AISI 316. The sodium side around the test pipe has been constructed as seven heat exchangers, as shown in Fig. 3 and the sodium is heated with an electric heater. The maximum available power in the Loop is 830 kW, including the power of the preheater. The test pipe has been very heavily instrumented [12, 13]. It will be sufficient to mention here that values of the inlet- and outlet temperature, the temperature along the test pipe at 9 m axial position, and of the pressure and mass flow both at the sodium and the water–steam-side have

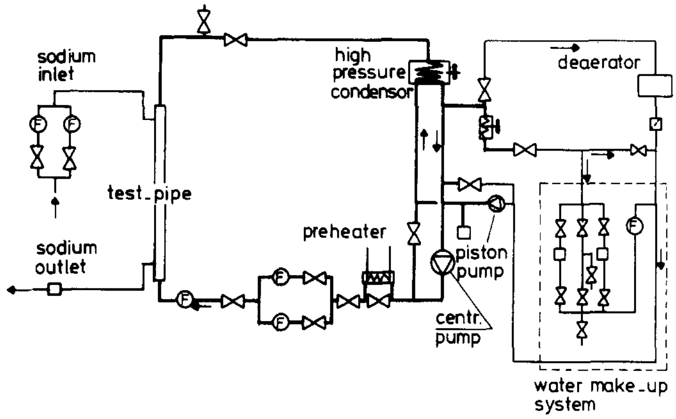

FIG. 2. Flow diagram of heat transfer loop.

been measured with pre-calibrated instruments. These data are collected with an on-line data acquisition system and processed by a Hewlett Packard-2216B computer.

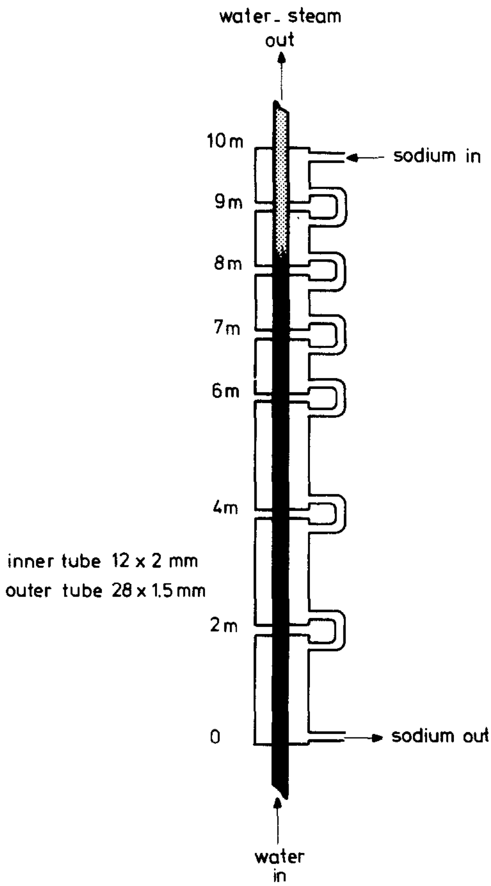

FIG. 3. Construction of sodium heated test pipe.

Water–steam-side temperatures have been measured with inconel sheathed, chromel–alumel thermocouples of 0.5 mm O.D. and the maximum error in determining the temperature and the difference between the temperatures at the inlet and outlet of the test pipe were calibrated as 1.2 and 0.6 K respectively.

Sodium-side temperatures have been measured with stainless steel sheated, chromel–alumel thermocouples of 0.5 mm O.D. and the maximum error in determining the temperature and the difference between the temperatures at the inlet and outlet of the test pipe were calibrated as 1.6 and 0.6 K respectively.

Both, water–steam-side and sodium-side mass flows have been measured with turbine flowmeters with an accuracy of less than 1%.

Water–steam-side outlet pressure has been measured with a dead-weight balance manometer with an accuracy of 0.03 MN/m^2.

During the tests demineralised water has been used with an oxygen content less than 15 ppb, with a conductivity less than 0.5 μS/cm and with a pH between 8.5 and 9.

The pictures of subcooled nucleate flow boiling have been taken through the cylindrical sapphire test section with a high-speed rotating-mirror camera (Dynafax, model 350) at a frequency of 5000 frames/s. During the experiments subcooling at the end of the test section was slowly decreased, while pressure, heat flux and mass velocity were kept constant. The objective of the camera could be adjusted such that the bubbles (or plugs) either in the whole cross-section or in half the cross-section of the cylindrical sapphire test section could be photographed. For every test run, pictures of boiling were taken with the two positions of the objective. It took half an hour to reach steady-state conditions after which photographs were taken. In total 42 runs have been carried out, which cover the following range of operating conditions:

$$P = 4.1\text{–}15.9\ \mathrm{MN/m^2}$$

$$G = 1869\text{–}2383\ \mathrm{kg/m^2\,s}$$

$$q = 0.10\text{–}0.50\ \mathrm{MW/m^2}$$

$$\Delta T_{sub} = 0.0\text{–}4.1\ \mathrm{K}$$

$$X = 0.0\text{–}2.9\,.$$

After developing the films, bubble (or plug) velocities and diameters were measured with a Boscar motion analyser in order to determine the weighted mean velocity of the vapour phase.

DETERMINATION OF THE WEIGHTED MEAN VELOCITY OF THE VAPOUR PHASE

Plug flow

At pressures lower than about 7 MN/m^2, plug flow started immediately after the initial point of net vapour generation, and a few plugs (or even sometimes a single plug) and several comparatively small bubbles in a liquid continuum were visible on the developed films, as shown schematically in Fig. 4. The magnitudes of

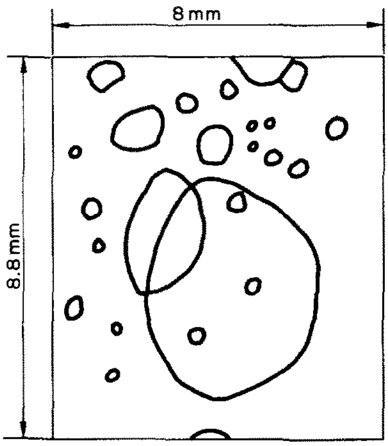

FIG. 4. Schematic description of plug flow at 4.1 MN/m^2.

the length and the diameter of a plug were in the same order of magnitude as the tube diameter. The velocity of every plug and bubble appearing on the film was measured in several axial positions (between 2 and 28 positions). Thus the number of velocities measured varied between 8 and 247 for each test run. The reason why the velocity of a plug or a bubble has been measured at several axial positions was to determine the time-averaged value of the velocity. As shown in the paper of Warschauer [12], the velocities of bubbles (or plugs) vary significantly with time during the bubble or (plug) flow regime.

Since all the bubbles and plugs were approximately elliptically shaped, the diameter of a plug (or bubble) was determined by averaging the measured major and minor axes of a plug (or bubble). No deformation in plug (or bubble) shape has been observed during measurement of the velocity of a plug (or bubble).

In order to determine the weighted mean velocity of the vapour phase (or velocity of the centre of gravity of the vapour phase in plug flow) the following equation has been used:

$$\bar{V}\frac{\pi}{6}\rho_v\sum_{e=1}^{e} D_e^3 = \frac{\pi\rho_v}{6}$$
$$\times\left(\frac{D_1^3}{m}\sum_{m=1}^{m} V_m + \frac{D_2^3}{m}\sum_{m=1}^{m} V_m + \ldots + \frac{D_e^3}{m}\sum_{m=1}^{m} V_m\right) \quad (18)$$

and it was possible to determine this velocity up to a void fraction of 33%. It follows from the description of the plug flow regime that the small bubbles which could not be seen on a developed film do not substantially affect the prediction of the weighted mean velocity of the vapour phase, since the bubble volume used in equation (18) is proportional to the third power of the bubble diameter, which is much smaller than the diameter of a plug.

Bubble flow

For pressures higher than about 10 MN/m^2, numerous small bubbles of different sizes in a continuous liquid were visible on the developed films up to high values of steam quality. Distribution of the bubble diameters approximated a normal distribution. Since the number of bubbles on a developed film was large, the weighted mean velocity of the vapour phase for this flow regime was determined by a statistical method from the measured velocities of a sufficient number of bubbles taken randomly from the bubble population. For each test run, a sample of 4 to 10 bubbles was taken from the bubble population and the velocity and diameter (or major and minor axes when they are elliptically shaped) of each bubble in the sample was measured at several axial positions (between 1 and 19 positions). Thus the number of velocities measured varied between 15 and 140 for each test run. Analysed bubble populations were selected such that a representative bubble sample could be taken from them. For this flow regime, it was possible to determine the weighted mean velocity of the vapour phase up to 18% void fraction, and this velocity has been calculated with the formula below:

$$\bar{V}=\frac{1}{f}\sum_{f=1}^{f}\left(\frac{1}{m}\sum_{m=1}^{m} V_m\right)_f \quad (19)$$

or

$$\bar{V}\frac{\pi}{6}\rho_v\sum_{f=1}^{f} D_f^3 = \frac{\pi\rho_v}{6}$$
$$\times\left(\frac{D_1^3}{m}\sum_{m=1}^{m} V_m + \frac{D_2^3}{m}\sum_{m=1}^{m} V_m + \ldots + \frac{D_f^3}{m}\sum_{m=1}^{m} V_m\right) \quad (20)$$

The weighted mean velocity of the vapour phase predicted by equation (19) has been considered for further analyses, since it was found to differ by not more than a few per cent from that predicted by equation (20).

DETERMINATION OF STEAM QUALITY

During the tests, heat losses were compensated by installing trace heaters in the insulation material which covered the sodium side. Steam quality has therefore been calculated from the following heat balance:

$$[W(t_i-t_0)c_p]_n-[W(H_0-H_i)]_w = W_w X r. \quad (21)$$

The specific heat of sodium and the properties of water have been taken from [14, 15].

Since the steam quality in the subcooled boiling region is comparatively low, the steam quality calculated with equation (21) may involve a considerable error. In order to minimise this error in steam quality, the following method was adopted: During the experiments, only the subcooling at the end of the test pipe was slowly decreased, while mass velocity, heat flux and pressure were kept constant. In this way first the initial point of net vapour generation was determined from the developed films, as explained in [16]. At this particular point steam quality can be considered to be negligibly low [17]. Thereafter subcooling was plotted versus $XW_w r$, the heat used for vapour formation for a given pressure, and the best fitting curve was drawn through the experimental points. An example of this is shown in Fig. 5, for 12 MN/m^2. Then for a given subcooling, $XW_w r$, the heat used for vapour formation was determined from the figure and from this the steam quality.

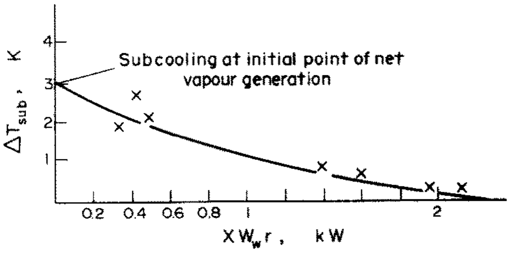

FIG. 5. Determination of steam quality at 12 MN/m^2.

Although the error in determining steam quality may be considerable, it does not introduce any significant error in the determination of J, the average volumetric flux density of the mixture, since steam quality varied up to 2.9% during all the test runs [see equation (11)].

CORRELATION OF DATA

In order to correlate the data by using equation (7), $\bar{V}$, the weighted mean velocity of the vapour phase, has been plotted vs J, the average volumetric flux density of the steam-water mixture, for a given pressure, as shown in Fig. 6, for example for 4.1 MN/m^2. The interception of the line drawn through the experimental data with the $\bar{V}$ axis gives V_d, the weighted mean drift velocity. As could be seen from the figure, the value of the distribution parameter is equal to 1 and that of weighted mean drift velocity equals 0.3 m/s. The distribution parameters and weighted mean drift velocities determined by this procedure for all test runs yield:

$$C = 1 \tag{22}$$

$$V_d = 0.36\,(1-P_r)^{0.9} \tag{23}$$

as shown in Fig. 7, and equations (7) and (9) become respectively:

$$\bar{V} = J + 0.36\,(1-P_r)^{0.9} \tag{24}$$

and

$$\beta/\bar{\alpha} = 1 + 0.36\,(1-P_r)^{0.9}/J. \tag{25}$$

Since $V_d/J \ll 1$ for the operating conditions of our tests, determination of the distribution (or flow) parameter seems fairly accurate and the value of this parameter is in contradiction with that reported in [3, 6].

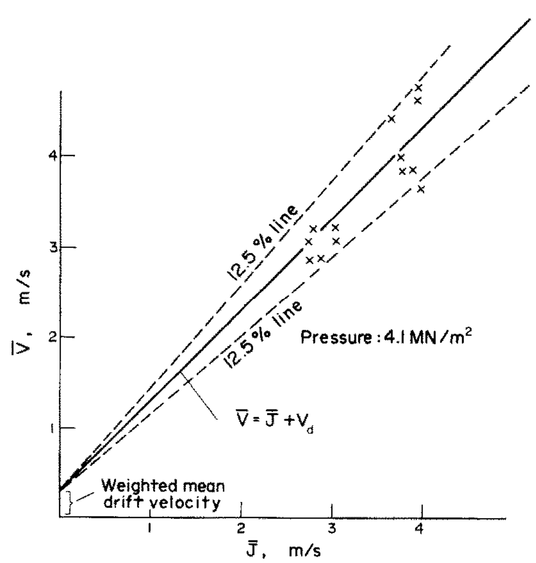

FIG. 6. Determination of distribution parameter and weighted mean drift velocity at 4.1 MN/m^2.

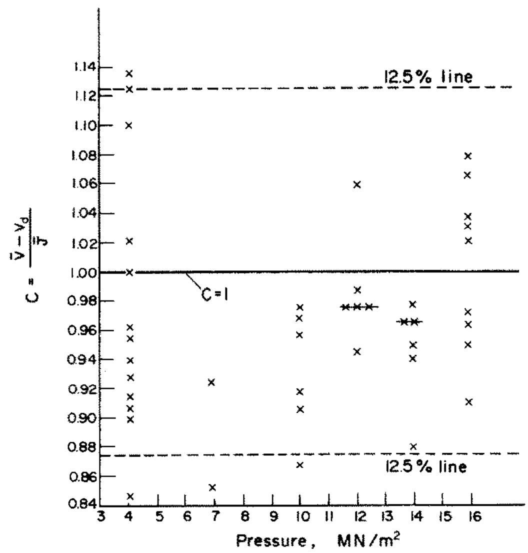

FIG. 7. Correlation of all data.

During our experiments, void fraction has not been measured. Therefore, in order to show the validity of equation (25) [and hence of equation (8)], this equation has been compared with extensive data of several investigators [18–21] taken for the saturated bulk boiling of water and for the flow of steam–water mixtures without heat addition in vertical circular tubes, annuli and rectangular channels, as shown in Figs. 8 and 9. The range of the data is summarised in Table 1. The number of data considered was 497. Not all the data from [18–21] could be included in these figures, however. The data shown in these figures have therefore been selected in such a way that the maximum spread of the value of the distribution parameter can be seen. Moreover, only the data from [19–21] for comparatively high steam qualities, as indicated in Table 1, have been studied, since for subcooled

Table 1. Conditions for void fraction experiments of various investigators

P (MN/m^2)	Number of data	Geometry	d_H (mm)	Heat flux (MW/m^2)	G (kg/m^2 s)	X (%)	α (%)	Reference
3–5	75	circular tube	9.16	adiabatic	388–3504	0–80	0–99	[18]
13.8	54	rectangular channel	4.74	0.32–1.58	895–1153	10–37.3	42–85	[19]
2–9.8	158	circular tube and annulus	7.7–10.2	adiabatic	400–3400	0–88	0–99	[20]
2–9.8	18	circular tubes	15.7–34.3	0.014–2	400–1700	5–60	30–99	[20]
2–5	192	annulus	13	0.60–1.22	652–1368	5.2–18.2	55–87	[21]

nucleate flow boiling, in which steam qualities are low, a simple heat balance does not give the steam quality due to the thermal non-equilibrium existing between the phases [7, 17, 22].

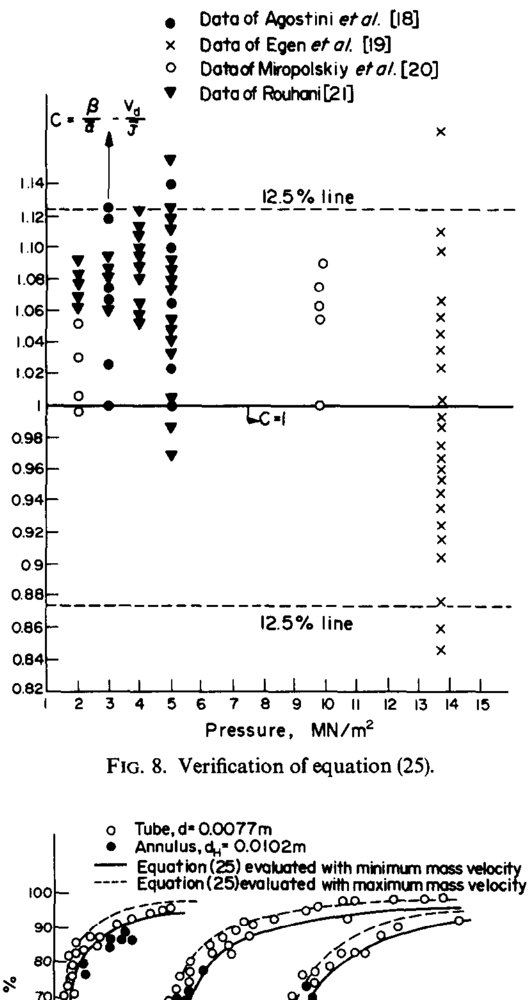

FIG. 8. Verification of equation (25).

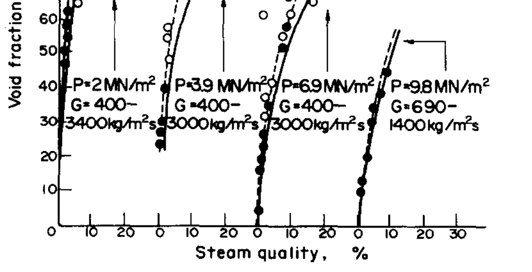

FIG. 9. Comparison of equation (25) with data of Miropolskiy *et al.* [20] from unheated channels.

It follows from Figs. 8 and 9 that equation (25) correlates the aforesaid data fairly well and that the value of the distribution parameter, which best fits the data is 1. For almost all these data, including those of the present work, $V_d/\bar{J} \ll 1$. What has been demonstrated above is sufficient evidence at the present state of art that both equations (24) and (25) and therefore equation (8) are valid, and that the value of the distribution (or flow) parameter is equal to 1 for the conditions considered in this study.

Equation (25) is recommended to predict the void fraction for these conditions, which are as follows:

Geometry: vertical pipes, vertical annuli and vertical rectangular channels;

P, 2–15.9 MN/m^2;
α, 0.00–99%;
d_H, 0.0047–0.0343 m;
G, 388–3500 kg/m^2 s;
q, adiabatic (without heat addition) and 0.01–2.0 MW/m^2.

For horizontal pipes, equation (25) reduces to $\beta/\bar{\alpha} = 1$ since $V_d = 0$. This equation fits, within 8.5% error limits, the correlation of Armand and Treshchev [2] based on data taken for the flow of steam–water mixtures with or without heat addition in horizontal pipes of 2.6 and 5.6 cm I.D., in the pressure range of 1–17.7 MN/m^2 and for steam qualities less than 0.9.

As can be seen from equation (25), $V_d/\bar{J}$ is much smaller than 1 for high mass velocities and pressures and the value of the weighted mean drift velocity given by equation (23) is in fact an average value for different types of channel geometry and flow pattern. Therefore, for the application of equation (25) to very low mass velocities, adequate information is needed for the values of the weighted mean drift velocity for different types of flow pattern and geometry, which are at present being measured in our Institute.

2. INCIPIENT POINT OF BOILING—INTRODUCTION AND EXPERIMENTAL DATA

During the subcooled nucleate flow boiling of a liquid in a channel, there is a point where the first bubble forms and gets detached from the heated surface. This point is termed Incipient Point of Boiling in the literature, and is of importance for the design of liquid-cooled reactors and steam generators since heat transfer rapidly increases beyond this point and bubbles begin to appear in the subcooled liquid.

Up to now, no direct method has been reported in literature for the determination of the IPB for the subcooled nucleate flow boiling of water [23–25], but with high-speed photography it has been found possible to determine this point directly. The experimental set-up used for this purpose is described in the first part. The pictures of subcooled nucleate flow boiling were taken at constant pressure, heat flux and mass velocity, while subcooling was decreased slowly. When the first bubble was seen on a developed film, the conditions at which the film was taken were specified as those of the IPB, as given in Table 2.

Table 2. Data for IPB

P (MN/m^2)	G (kg/m^2 s)	q (MW/m^2)	ΔT_{sub} K	D_d (mm)
15.9	2134	0.391	7.3	0.225
14.0	2167	0.336	6.9	0.255
12.0	2208	0.326	5.9	0.300
10.0	2040	0.138	2.6	0.313
4.1	2189	0.128	2.9	0.210

At the IPB, two or three bubbles were visible on a developed film and they were either spherically or elliptically shaped. Bubble diameters were measures from a developed film with a Boscar motion analyser and averaged over the number of bubbles seen on the film (see Table 2). When a bubble was elliptically shaped, the bubble diameter was determined by averaging the measured major and minor axes of the bubble.

The heat flux at the IPB (i.e. at the end of the test pipe) has been calculated from the following formula:

$$q = (t_i - T_0)U \tag{26}$$

where U has been determined from the heat balance for the last metre of the test pipe, i.e.

$$U = \frac{[Wc_p(t_i - t_z)]_n}{\pi d}\left\{\frac{(t_i - T_0) - (t_z - T_z)}{\ln\dfrac{t_i - T_0}{t_z - T_z}}\right\}^{-1}. \tag{27}$$

CORRELATION OF DATA FOR THE IPB

In order to correlate the IPB data, the following heat transfer equation for subcooled nucleate flow boiling, derived by the author of this paper, has been used [16]:

$$q = C_1 \Delta T_{sat}^n + h\,\Delta T_{sub} \tag{28}$$

where

$$C_1 = \frac{\mu_1 r\left(\dfrac{c_p}{0.013 r\,Pr^{1.7}}\right)_1^3}{\left(\sigma/[g(\rho_1 - \rho_v)]\right)^{1/2}} \tag{29}$$

$$n = 3. \tag{30}$$

The heat flux at the IPB can be given by equation (28):

$$q_I = C_1(\Delta T_{sat})_I^n + h_I(\Delta T_{sub})_I. \tag{31}$$

For a constant heat flux system, the following equation applies to fully developed boiling [26–28]:

$$q_I = C_1(\Delta T_{sat})_F^n. \tag{32}$$

Equation (31) can be reduced to a non-dimensional form by the use of equation (32):

$$\left(\frac{h\,\Delta T_{sub}}{q}\right)_I = \left(1 - \frac{(\Delta T_{sat})_I^n}{(\Delta T_{sat})_F^n}\right). \tag{33}$$

It has been shown in [16] that the term in parentheses on the LHS of equation (33) is a constant at the initial point of net vapour generation regardless of operating conditions and channel geometry; it is equal to 0.24

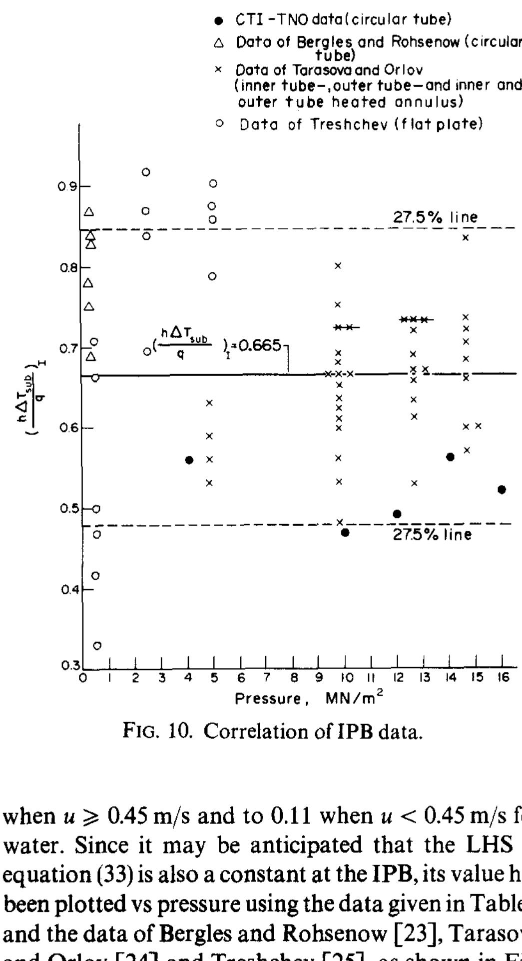

FIG. 10. Correlation of IPB data.

when $u \geqslant 0.45$ m/s and to 0.11 when $u < 0.45$ m/s for water. Since it may be anticipated that the LHS of equation (33) is also a constant at the IPB, its value has been plotted vs pressure using the data given in Table 2 and the data of Bergles and Rohsenow [23], Tarasova and Orlov [24] and Treshchev [25], as shown in Fig. 10. The forced convection heat transfer coefficient in the LHS of equation (33) has been evaluated with the well-known correlation $Nu_b = C_2 Re_b^{0.8} Pr_b^{0.4}$, in which C_2 equals 0.023 for circular tubes [29] and 0.015 $(d_2/d_1)^{0.25}$ for inner tube-, outer tube- and inner and outer tube heated annuli [30]. For a flat plate, the forced convection heat-transfer coefficient has been predicted with the formula $Nu = 0.0366\,Re^{0.8}\,Pr^{1/3}$, in which the fluid properties have to be determined at the temperature given below [29]:

$$T = T_b - \frac{0.1\,Pr + 40}{Pr + 72}(T_b - T_s). \tag{34}$$

As for the data of Bergles and Rohsenow [23], the forced convection heat-transfer coefficient given in their paper has been used. It follows from Fig. 10

$$\frac{h_l(\Delta T_{sub})_l}{q_l} = 0.665 \tag{35}$$

regardless of channel geometry and operating conditions.

Equation (35) is valid for a wide range of conditions:

Geometry: plate, circular tube, and inner tube-, outer tube—and inner- and outer tube heated annulus;

P, 0.15–15.9 MN/m^2;
G, 470–17355 kg/m^2 s;
q, 0.13–9.8 MW/m^2;
ΔT_{sub}, 2.6–108 K;
d_H, 0.00239–0.032 m;

material of heating surface: stainless steel and nickel.

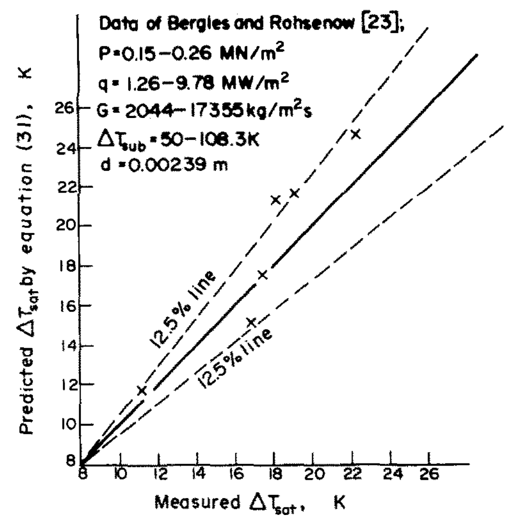

FIG. 11. Correlation of superheating data of Bergles and Rohsenow [23].

SUPERHEATING AT THE IPB

Only few data for superheating at the IPB during the subcooled nucleate flow boiling of water have been found in the paper of Bergles and Rohsenow [23]. As demonstrated in [31], the degree of superheating at the IPB cannot be determined from the formula $q_l = h_l(T_s - T_b)_l$.

In order to correlate the superheating data of Bergles and Rohsenow taken in a stainless steel circular tube [23], the heat-transfer correlation for subcooled nucleate flow boiling given by equation (31) has been used, as shown in Fig. 11. Equation (31) correlates the superheating data of the aforesaid investigators very well.

MAXIMUM BUBBLE DIAMETER AT THE IPB

In order to correlate the data for maximum bubble diameter (or bubble departure diameter) at the IPB the correlation derived by the author to determine the maximum bubble diameter of a subcooled nucleate flow boiling bubble has been modified [32]. The aforesaid correlation is based on a heat-transfer controlled bubble model and is valid for the determination of the maximum diameter of the average bubble of a bubble population consisting of numerous bubbles. At the IPB there exist few bubbles, and the growth of a bubble is thus not affected by liquid agitation caused by movement of the numerous bubbles, in contradiction with the growth of a bubble in a bubble population. The effect on bubble growth of liquid agitation caused by the movement of numerous bubbles has been given as a function of pressure in [32]. The correlation given in [32] has therefore been modified only by altering the numerical constant and pressure term in it by using the data given in Table 2 and the data of Abdelmessih *et al.* [33] taken from an artificial nucleation site manufactured from stainless steel, as shown in Fig. 12 and given below:

$$D_d = 1.725\ 10^{-7}\, a(b\Phi)^{-1/2} P^{1.072} \tag{36}$$

where

$$a = \frac{\Delta T_{sat} k_l [k_s \rho_s c/(k\rho c_p)_l]^{1/2}}{2\rho_v r[\pi k/(\rho c_p)]_l^{1/2}} \tag{37}$$

$$b = \frac{\Delta T_{sub}}{2(1-\rho_v/\rho_l)} \tag{38}$$

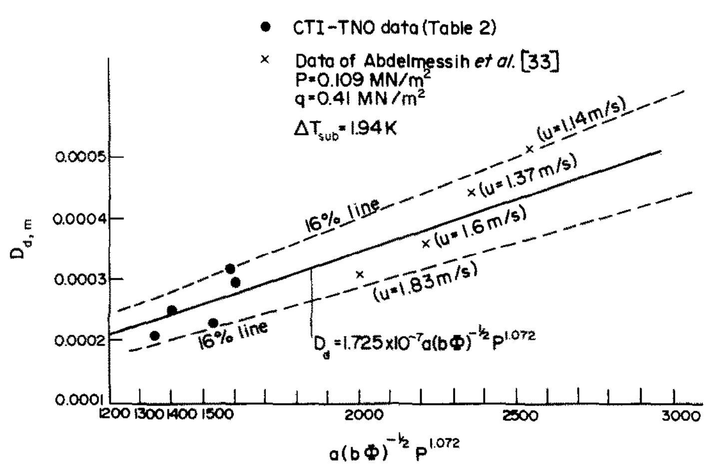

FIG. 12. Correlation of the data for maximum bubble diameter at the IPB.

$$\Phi = \left(\frac{u}{u_0}\right)^{0.47} \quad \text{for} \quad u > 0.61\ \text{m/s} \tag{39}$$

$$\Phi = 1 \quad \text{for} \quad u \leqslant 0.61\ \text{m/s} \tag{40}$$

$$u_0 = 0.61\ \text{m/s}. \tag{41}$$

For data given in Table 2 the superheating has been evaluated with equation (31). For the data of Abdelmessih *et al.* [33] the superheating given in their paper has been used. In order to predict the properties of stainless steel, type 304 (austenitic) 18-8S has been considered. Properties of water have been taken from [15].

Acknowledgement—This study has been performed under the auspices of the Project Group for Nuclear Energy TNO. The author wishes to thank Mr. K. A. Warschauer and Mr. M. L. G. van Gasselt for their encouragement during the preparation of this work, and to Mr. P. H. Engelman, Mr. W. van Deelen and Mr. P. J. de Munk, who at an earlier stage were in charge of the construction of the test facilities and in conducting the experiments.

REFERENCES

1. A. A. Armand, The resistance during the movement of a two-phase system in horizontal pipes, AERE-Trans 828 (1959).
2. A. A. Armand and G. G. Treshchev, Investigation of the resistance during the movement of steam–water mixtures in a heated boiler pipe at high pressures, AERE Lib/Trans 816 (1959).
3. S. G. Bankoff, A variable density single-fluid model for two-phase flow with particular reference to steam–water flow, *J. Heat Transfer* **82**, 265–272 (1960).
4. N. Zuber and J. A. Findlay, Average volumetric concentration in two-phase flow systems, *J. Heat Transfer* **87**, 453–468 (1965).
5. F. W. Staub and N. Zuber, Void fraction profiles, flow mechanisms and heat transfer coefficients for Refrigerant 22 evaporating in a vertical tube, *Proceedings of the ASHRAE Semiannual Meeting*, 24–27 *January* 1966, *Houston, Texas*, pp. 130–146 (1966).
6. N. Zuber, F. W. Staub and G. Bijwaard, Vapor void fraction in subcooled boiling systems, *Proceedings of the Third International Heat Transfer Conference*, 7–12 *August* 1966, *Chicago*, Illinois, Vol. 5, pp. 24–38. AIChE, New York (1966).
7. P. G. Kroeger and N. Zuber, An analysis of the effects of various parameters on the average void fractions in subcooled boiling, *Int. J. Heat Mass Transfer* **11**, 211–233 (1968).
8. N. Adorni, G. Peterlongo, R. Ravetta and F. A. Tacconi, Large scale experiments on heat transfer and hydrodynamics with steam–water mixtures: phase and velocity distribution measurements in a round vertical tube, CISE-R-91 (1964).
9. A. Inoue, S. Aoki and T. Koga, On the void and the velocity profiles of two-phase bubble flow in a vertical pipe, Presentation made at the Round Table Discussion on Momentum and Heat Transfer Mechanisms in Two-Phase Flow, Fifth International Heat Transfer Conference, Tokyo (3–7 September 1974).
10. K. Kobayasi, Measuring method of local phase velocities and void fraction in bubbly and slug flows, Presentation made at the Round Table Discussion on Momentum and Heat Transfer Mechanisms in Two-Phase Flow, Fifth International Heat Transfer Conference, Tokyo (3–7 September 1974).
11. K. Ohba, Simultaneous measurement of local flow velocity and void fraction in bubbly flows using a gas laser, Presentation made at the Round Table Discussion on Momentum and Heat Transfer Mechanisms in Two-Phase Flow, Fifth International Heat Transfer Conference, Tokyo (3–7 September 1974).
12. K. A. Warschauer, Model testing and heat transfer research at TNO for the design and development of sodium cooled steam generators and other heat extraction equipment, Proceedings of the Information Meeting—TNO Contribution to LMFBR Development, Utrecht, Netherlands, pp. 68–78 (10–11 May 1973).
13. P. J. de Munk, Two-phase flow experiments in a 10 m long sodium heated steam generator test section, Proceedings of International Meeting on Reactor Heat Transfer, Karlsruhe, pp. 504–518 (9–11 October 1973).
14. M. E. Durham, The thermodynamic and transport properties of liquid sodium, CEGB-Report-RD/B/M2479 (Revised)—CFR/THWP/P(72) 28 (Revised) (1974).
15. The American Society of Mechanical Engineers, *1967 ASME Steam Tables*, New York (1967).
16. H. C. Ünal, Determination of the initial point of net vapor generation in flow boiling systems, *Int. J. Heat Mass Transfer* **18**, 1095–1099 (1975).
17. S. Levy, Forced convection subcooled boiling-prediction of vapor volumetric fraction, *Int. J. Heat Mass Transfer* **10**, 951–965 (1967).
18. G. Agostini, A. Era and A. Premoli, Density measurements of steam-water mixtures flowing in a tubular channel under adiabatic and heated conditions, *Energia Nucl., Milano* **18**, 295–310 (1971).
19. R. A. Egen, D. A. Dingee and J. W. Chastain, Vapor formation and behaviour in boiling heat transfer, BMI 1163 (1957).
20. Z. L. Miropolskiy, R. I. Shneyerova and A. I. Karamysheva, Vapor void fraction in steam–fluid mixtures flowing in heated and unheated channels, Preprints of papers presented at the Fourth International Heat Transfer Conference, Paris–Versailles 1970, *Heat Transfer 1970*, Vol. 5, Paper No. B4.7 (1970).
21. S. Z. Rouhani, Void measurements in the regions of subcooled and low-quality boiling, AE-239, Aktiebolaget Atomenergi, Stockholm, Sweden (1966).
22. S. Z. Rouhani and E. Axelsson, Calculation of void volume fraction in the subcooled and quality boiling regions, *Int. J. Heat Mass Transfer* **13**, 383–393 (1970).
23. A. E. Bergles and W. M. Rohsenow, The determination of forced convection surface-boiling heat transfer, *J. Heat Transfer* **86**, 365–372 (1964).
24. N. V. Tarasova and V. M. Orlov, Heat transfer and hydraulic resistance during surface boiling of water in annular channels, in *Convective Heat Transfer in Two-Phase and One-Phase Flows*, edited by V. M. Borishanskii and I. I. Paleev, pp. 135–156. Israel Program for Scientific Translations, Jerusalem (1969).
25. G. G. Treshchev, The number of vapor formation centers in surface boiling, in *Convective Heat Transfer in Two-Phase and One-Phase Flows*, edited by V. M. Borishanskii and I. I. Paleev, pp. 97–105. Israel Program for Scientific Translations, Jerusalem (1969).
26. K. E. Forster and R. Greif, Heat transfer to a boiling liquid-mechanism and correlations, *J. Heat Transfer* **81**, 43–53 (1959).
27. S. S. Kutateladze, Boiling heat transfer, *Int. J. Heat Mass Transfer* **4**, 31–45 (1961).
28. W. M. Rohsenow, A method of correlating heat-transfer data for surface boiling of liquids, *Trans. Am. Soc. Mech. Engrs* **74**, 969–976 (1952).
29. J. G. Knudsen and D. L. Katz, *Fluid Dynamics and Heat Transfer*, p. 394 and pp. 485–486. McGraw-Hill, New York (1958).
30. S. S. Kutateladze and V. M. Borishanskii, *A Concise Encyclopedia of Heat Transfer*, p. 114. Pergamon Press, Oxford (1966).
31. A. H. Abdelmessih, S. T. Yin and A. Fakhri, Hysteresis

effects and hydrodynamic oscillations in incipient boiling of Freon 11, in *Proceedings of International Meeting on Reactor Heat Transfer, Karlsruhe*, October 9–11, 1973, pp. 331–350 (1973).

32. H. C. Ünal, Maximum bubble diameter, maximum bubble-growth time and bubble-growth rate during the subcooled nucleate flow boiling of water up to 17.7 MN/m^2, *Int. J. Heat Mass Transfer* **19**, 643–649 (1976).
33. A. H. Abdelmessih, F. C. Hooper and S. Nangia, Flow effects on bubble growth and collapse in surface boiling, *Int. J. Heat Mass Transfer* **15**, 115–125 (1972).

FRACTION DE VIDE ET POINT DE DEBUT D'EBULLITION POUR L'EBULLITION NUCLEEE SOUS-REFROIDIE DANS L'ECOULEMENT DE L'EAU

Résumé—On a déterminé la fraction de vide au moyen de la photographie ultra-rapide pour l'ébullition nucléée sous-refroidie dans l'écoulement de l'eau. Les données obtenues ainsi que celles d'autres auteurs relatives à l'écoulement adiabatique d'un mélange d'eau et de vapeur d'eau et à l'ébullition saturée de l'eau ont conduit à une corrélation qui s'applique aux conditions suivantes.

Géométrie: tubes verticaux circulaires; canaux rectangulaires et annulaires; pression 2–15,9 M N/m^2; vitesse massique 388–3500 kg/m^2 s; fraction de vide 0–99 pour cent; diamètre hydraulique 0,0047–0,0343 m; flux de chaleur: adiabatique de 0,01–2,0 M W/m^2; précision: 12,5 pour cent.

La valeur du paramètre dit de distribution (ou d'écoulement) a été déterminée expérimentalement et trouvée égale à 1 pour un tube vertical circulaire de faible diamètre.

Le point de début d'ébullition pour l'ébullition nucléée sous-refroidie dans l'écoulement de l'eau a été déterminé à l'aide de la photographie ultra-rapide. Les données obtenues et les données disponibles dans la littérature ont conduit à une corrélation valable pour les conditions suivantes.

Géométrie: plaque, tube circulaire et annulaire avec tubes chauffés à l'intérieur seulement, à l'extérieur seulement ou à l'intérieur et à l'extérieur; pression: 0,15–15,9 M N/m^2; vitesse massique 470–17355 kg/m^{2}s; diamètre hydraulique 0,00239–0,032 m; flux de chaleur: 0,13–9,8 M W/m^2; sous-refroidissement: 2,6–108 K, matériel de la surface chauffée: acier inoxydable et nickel; précision: 27,5 pour cent.

Les diamètres maximaux des bulles ont été mesurés au point de début d'ébullition. Ces données et celles disponibles dans la littérature ont été corrélées pour le domaine de pression de 0,1 à 15,9 M N/m^2.

DAMPFVOLUMENANTEIL UND STELLE ERSTER BLASENBILDUNG WAEHREND DER UNTERKUEHLTEN SIEDESTROEMUNG VON WASSER

Zusammenfassung—Der Dampfvolumenanteil für die unterkühlte Siedeströmung von Wasser ist mittels ultraschneller Fotografie bestimmt worden. Die erhaltenen Daten und die Daten von verschiedenen Forschern für adiabatische Dampf-Wasser Gemischen und für gesättigtes Sieden des Wassers haben eine Korrelation im folgenden Bereich erbracht: Geometrie: vertikale, kreisrunde Rohre, rechtwinklige Kanäle und Spalte; Druck: 2–15,9 MN/m^2, Massengeschwindigkeit: 388–3500 kg/m^2 s; Dampfvolumenanteil: 0–99 Prozent; hydraulischer Durchmesser: 0,0047–0,0343 m; Wärmestromdichte: adiabatisch und 0,01–2,00 MW/m^2; Genauigkeit: 12,5 Prozent.

Der sogenannte Verteilungs- (oder Strömungs-) parameter ist experimentell bestimmt worden, und zwar ist er gleich 1 für ein vertikales kreisrundes Rohr mit kleinem Durchmesser.

Die Stelle der ersten Blasenbildung für unterkühlte Siedeströmung des Wassers ist mittels ultraschneller Fotografie bestimmt worden. Die erhaltenen Daten und die in der Literatur zur Verfügung stehenden Daten haben zu einer Korrelation geführt, die für die folgenden Bedingungen gilt: Geometrie: Platte, kreisförmige Rohre und ringförmige Spalte von innen, von aussen und sowohl innen als aussen beheizt; Druck: 0,15–15,9 MN/m^2; Massengeschwindigkeit: 470–17355 kg/m^2 s; hydraulischer Durchmesser: 0,00239–0,032 m; Wärmestromdichte: 0,13–9,8 MW/m^2; Unterkühlung: 2,6–108 K; Werkstoff der Heizoberfläche: rostfreier Stahl und Nickel; Genauigkeit: 27,5 Prozent.

Die maximalen Blasendurchmesser sind an der Stelle der ersten Blasenbildung gemessen worden. Diese Daten und die Daten aus der Literatur sind für den Druckbereich von 0,1 bis 15,9 MN/m^2 korreliert worden.

ОБЪЕМНОЕ ПАРОСОДЕРЖАНИЕ И ВОЗНИКНОВЕНИЕ ПУЗЫРЬКОВОГО КИПЕНИЯ В ПОТОКЕ НЕДОГРЕТОЙ ЖИКДОСТИ

Аннотация — Объемное паросодержание определялось путем высокоскоростного фотографирования во время пузырькового кипения в потоке недогретой воды. Полученные результаты и литературные данные по адиабатическому потоку пароводяных смесей и кипению насыщенной воды в большом объеме были обобщены для следующих условий: геометрия: вертикально направленные круглые трубки, прямоугольные и кольцевые каналы; давление: 2–15,9 Мн/м^2; массовая скорость: 388–3500 кг/м^2 сек; объемное паросодержание: 0–99%; диаметр потока: 0,0047–0,0343; тепловой поток; адиабатический и 0,01–2,0 Мвт/м^2. Точность критериальных уравнений составляла 12,5%. Величина так называемого параметра распределения была экспериментально найдена равной единице для вертикальной круглой трубки с небольшим диаметром. Возникновение пузырькового кипения в потоке недогретой воды определялось с помощью высокоскоростного фотографирования. Полученные результаты и имеющиеся литературные данные были прокоррелированы для следующих условий: геометрия: пластина, круглые трубки и кольцевые трубки с внутренним, внешним и одновременно внутренним и внешним нагревом; давление: 0,15–15,9 Мн/м^2; массовая скорость: 470–173 551 кг/м^2 сек; гидравлический диаметр: 0,00239–0,032 м; тепловой поток: температура недогрева: 2,6–108 К; материал обогреваемой поверхности: нержавеющая сталь и никель. Точность обработки — 27,5%. Максимальные диаметры пузырьков измерялись в момент возникновения кипения. Эти результаты и литературные данные были прокоррелированы для диапазона давления от 0,1 до 15 Мн/м^2.